Journal of Engineering and Applied Sciences 14 (11): 3813-3831, 2019
ISSN: 1816-949X

Dynamic Modelling and Simulation of Grid Coupled DFIG Designed for 2 MW SHPP using ANN Scheme

Sanjeev Kumar Gagrai, Sundram Mishra and Madhu Singh
Department of Electrical Engineering, National Institute of Technology, Jamshedpur,
P.O. NIT Jamshedpur, 831014 Jharkhand, India

Abstract: Traditionally fixed speed drives are commonly used in small hydro power plants. With the development power electronics converter an autonomous variable speed drives, i.e., Doubly Fed Induction Generator (DFIG) came into the fashion. Small hydropower plant as an alternative source of energy plays a vital role in altering the face of any developing country in terms of environment protection, economic growth and energy crisis. The focal motive of this proposed research work is to implement the advanced control strategy, i.e., Artificial Neural Network (ANN) in grid-connected Doubly Fed Induction Generator (DFIG) associated with Small Hydro Power Plant (SHPP). The proposed control scheme regulates both sides of converter, i.e., converter of grid side and rotor side and maintains the power factor at unity level in the grid side for diminishing the loss as well as regulating the effectual real and reactive power flow in the rotor side. With the assistance of DFIG, optimum real and reactive power flow from the rotor side to grid side occurs at an inconstant speed, i.e., super synchronous, synchronous and sub-synchronous speed. Along with this, controller of the grid side also maintains the DC bus voltage at a constant level for proper operation of rotor side as well as grid side. A 2 MW DFIG associated with 2 MW SHPP Model is simulated in Simulink for time domain applications. The system is stable under different load conditions and it is investigated with the help of model and simulations result. The ANN controller improves the dynamic response of DFIG and makes the system more apposite for real-time applications.

Key words: Artificial Neural Network (ANN), controller, Doubly Fed Induction Generator (DFIG), Grid Side Converter (GSC), Rotor Side Converter (RSC), utility grid

INTRODUCTION

In the ongoing era for sustainable development of any developing country, electrification plays a significant role. The necessity of energy consumption is growing swiftly day by day for human society's growth. Because of plentiful gains of electrical energy, its plea is increasing speedily, so for, achieving the energy crisis we have to utilize the renewable energy sources effectually and proficiently (Mishra *etal*., 2015). For making sustainable policies and for achieving high GDP progress in upcoming next 5 years, renewable energy based technologies is very much essential. Along with other renewable energy sources like solar energy, biogas, ocean energy, Geothermal energy, hydropower also plays a vital role to meet the energy crisis. In a small-scale view, hydel power is considered one of the supreme profitable energy technologies for bucolic electrification in developing countries (Mishra *etal*., 2015). Ministry of New and Renewable Energy (MNRE) efficiently developed small hydropower plant and the guesstimate of MNRE is about 20 GW. Recently, India is on its path to reaching the 175 GW mark for installed nonconventional energy by 2022 (Anonymous, 2017). So, for achieving this mark of 175 GW, the generation of electricity form small hydropower Plant is very much essential. The state-wise estimated potential of a hydropower project in India is as presented in "Fig. (1)" (Anonymous, 2017).

If, we are talking about overall world electricity generation then alone small hydropower plant (<10 MW) currently contributes 40 GW of whole electricity generation and also try to increase the installed capacity over 100 GW in coming years (Khan, 2015a, b). One of the main attribute of SHPP that it can generate electricity from running water of small rivers. In other words, it can also say that it dost not requires large size dams as well as the stored water. Small Hydro Power Plant (SHPP) is not associated with problems like as colonization, deforestation and building of dams as large hydropower plant contains these problems (Khan, 2015a, b). SHPP is very much beneficial to the environment along with its continuously reducing the habitude of the non-renewable fuel sources. It is best suited for the generation of electricity in inaccessible and secluded areas as well as it is free from high generation cost. There are numerous motives of implementing SHPP as a prime basis of

Corresponding Author: Sanjeev Kumar Gagrai, Department of Electrical Engineering, National Institute of Technology, Jamshedpur, P.O. NIT Jamshedpur, 831014 Jharkhand, India

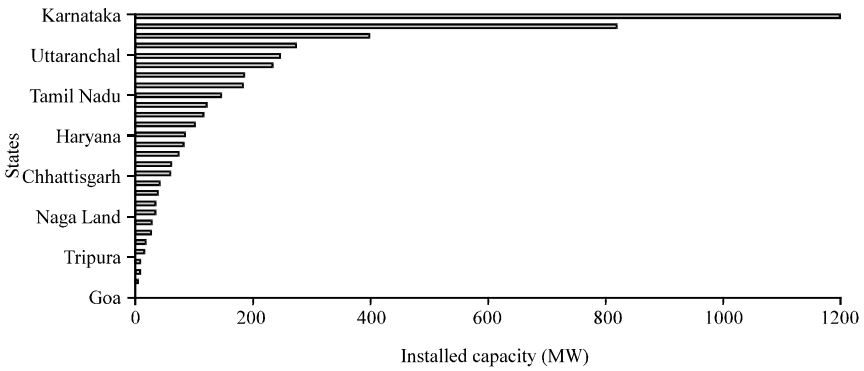

Fig. 1: Graphical representation of the estimated potential of SHP scheme in India; State wise estimated potential of small hydro power projected

generating electricity like as climate amiable, cost effective, unpolluted and reservoirs can also assist for water scarcity for irrigation intention and at the time of water supply scarcities (Anonymous, 2017; Khan, 2015a, b). All above-deliberated attributes make the small hydropower plant more and more eye-catching. In the current era, the requirement of high capacity hydropower plant with superior efficiency and fewer cost of generation is undoubtedly acceptable but these types of plant need special controllability requirement. So, for the goodness of environment and economy, the use of small-scale hydropower plant is increasing day by day (REN21., 2015). In this research work, we are using a Doubly Fed Induction Generator (DFIG) for adjustable speed control in SHPP. DFIG has already implemented in Wind Energy Conversion System (WECS) successfully. The construction view of DFIG is similar to slip ring induction machine or wound rotor induction machine and it works both as generator and motor. Here, we are employing as a generator with Small Hydro Power Plant (SHPP) due to its appreciating and eye-catching behavior. DFIG has several pros which make it more attractive which are given (Iov *et al*., 2008):

- DFIG has self-starting nature and it contains the three-phase supply for excitation purpose
- It generates the power from rotor as well as stator circuit under the condition of speed greater than synchronous speed
- The controlling nature of DFIG plays a significant role in the partial load operation
- It has good stability performance and faster response
- It reduces the oscillation in real power

For controlling purpose Artificial Neural Network (ANN) controller is employed for DFIG and DFIG is connected to the variable speed hydraulic turbine. The reasons for using the ANN controller because of its numerous advantages over the other controller techniques which are given (Ghumman *et al*., 2011). The effectiveness of the ANN on the stabilization of the system is very much good. The processing of the ANN becomes very simple due to the reduction of computational complication. One of the prime advantage of ANN is that it doesn't require any mathematical model, so, the requirement of time for computation is very much reduced (Soares *et al*., 2009). It contains a control unit which monitors all the activities of computing. The ANN-based controller improves the transient performance of the DFIG. Using the ANN approach this research work realizes real-time optimization because the optimization of this controller is done in real-time according to various real points (Haykin, 1998). The intention of this research work to effectively applied ANN controller and extracting the maximum hydropower. ANN controller improves the system transient performance of DFIG and due to this system can attain the reference speed more quickly in addition to controls the real and reactive power in the wide ambit of speed.

Table1: Categorization of SHPP on the basis of installed capacity (MW)

Types of Small Hydropower Plant (SHPP)	Installed capacity (MW)
Pico	0.005
Micro	>1
Mini	1-5
Small	>15

Description of SHPP: Due to unavailability of a global accord on definitions about small hydropower plant, generally because of diverse growth strategies in different countries. On the bases of installed capacity of hydropower projects, categorization of hydropower varies differently in numerous countries. A general classification of small hydropower plant is tabulated in "Table 1" (Mishra *et al*., 2015).

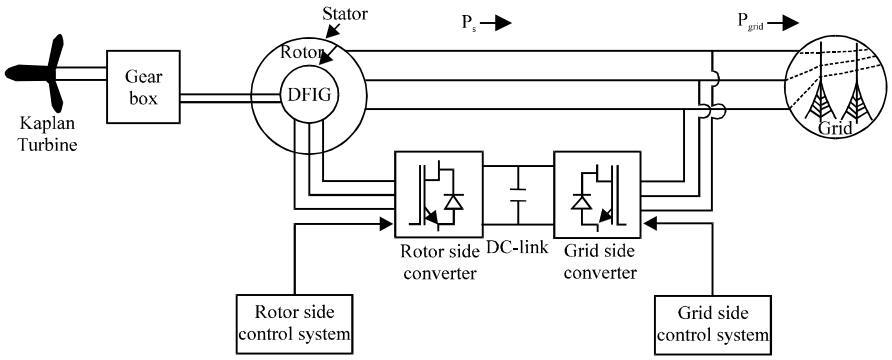

Fig. 2: Pictorial representation of back to back power converters with DFIG in SHPP system

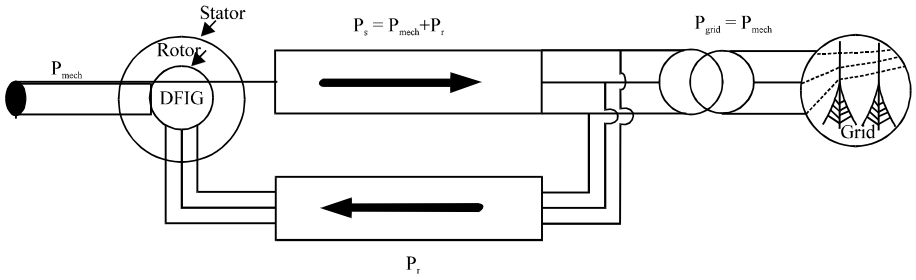

Fig. 3: Pictorial representation of power flow at sub-synchronous speed

enerally speaking, SHPP is a run-off-river type plant, so, it doesn't need any reservoir to store the water. Here, electricity is generated directly from the running water (Perez *et al*., 2008). The purpose of the hydraulic turbine to capture the water power and convert it to rotational power mechanically and Doubly Fed Induction Generator (DFIG) fed this rotational power as hydraulic turbine and DFIG is mechanically coupled together (Kothandaraman and Rudramoorthy, 2007). Basically, the efficiency of hydraulic turbine depends mainly on three-factor, i.e., the type of hydraulic turbine, the power capacity of the turbine and the amount of the fluid. As SHPP comes in the low head (<10 m) classification of hydropower plant (Angela, 2008). So, in the low head plant, Kaplan turbine is very much suitable due to its high efficiency (more than 90%) and another reason of using Kaplan turbine because it is most apposite for runoff river plant (Subramanya, 2013). The basic expression of generating power from hydropower plant depends on four major factors, i.e., the acceleration of the ground, the rate of water flow, turbine head and general efficiency. The basic expression of the generating power is displayed in "Eq. 1" (Borges and Pinto, 2008):

$$P = \eta_h Q_w \rho H_t g \quad (1)$$

Where:

P = Generated hydropower (kW)
g = Acceleration of gravity (m/sec^2)
Q_w = Rate of water flow (m^3/sec)
H_t = Head of the turbine (m)
η_h = General efficiency
ρ = Density of the water (g/cm^3)

Description of DFIG linked with SHPP: DFIG is very popular in wind energy application due to its economical pros for variable speed application. The same concept of DFIG can be used in SHPP as SHPP generates electricity from the running water (Boldea, 2005). The pictorial arrangement of DFIG associated with SHPP is shown below in "Fig. 2 and 3" (Madawala *et al*., 2012). In this converter system which is presented in "Fig. 2", rotor fed converter is called a Rotor Side Converter (RSC) and stator fed converter is known as Grid Side Converter (GSC). Both the converter is linked by the means of a link which is known as DC-link. The prime focus of the rotor side converter is to control the real and reactive power and this controllability of useful and reactive power is totally independent of the bidirectional power flow. Along with this grid side converter maintains the voltage at a constant level across the DC-link (Madawala *et al*., 2012).

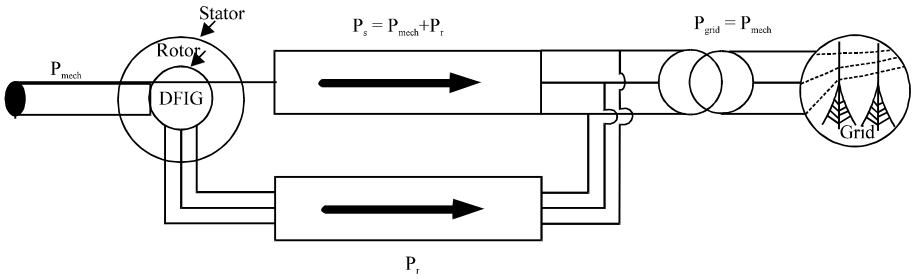

Fig. 4: Pictorial representation of power flow at super-synchronous speed

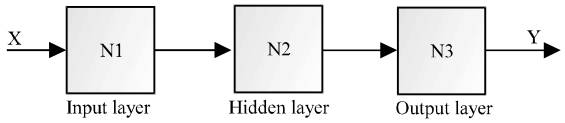

Fig. 5: Schematic representation of a three-layered MNN

In the above given "Fig. 2" DFIG is coupled to the grid via. two power converter (back to back) and it is also linked with Kaplan turbine viva gearbox which helps to maintain the speed arrangement amid turbine and rotor because the speed of rotor and turbine are different. The power flow between the rotor circuit and grid is known as slip power which totally depend on the slip. In the first case as given in "Fig. 3" (Magureanu *et al*., 2008) when DFIG works in sub-synchronous speed then the value of slip is positive then the whole amount of power supplied to machine stator which originates from rotor side as well as mechanical shaft also (Magureanu *et al*., 2008). In the second case as given in "Fig. 4 and 5" (Krishnan, 2001) when DFIG works in super synchronous mode then the value of the slip is negative then the power is delivered by the mechanical shaft to the stator and also to the rotor circuit (Krishnan, 2001). In a concise manner, we can say that in the case of the super-synchronous modeof operation, the direction of slip power will be from the rotor to the grid and in the case of the sub-synchronous mode of operation, the direction of slip power will be from grid to rotor. Therefore, the power converter which builds in back to back manner become essential due to their bi-directional action capability.

An overview of ANN: Among all the control learning model, ANN is the most powerful. It contains the attributes for approximating an extensive ambit of non-real functions which represent multidimensional input-output mapping. Neural networks have ingrained adaptability and can execute robust performance in the

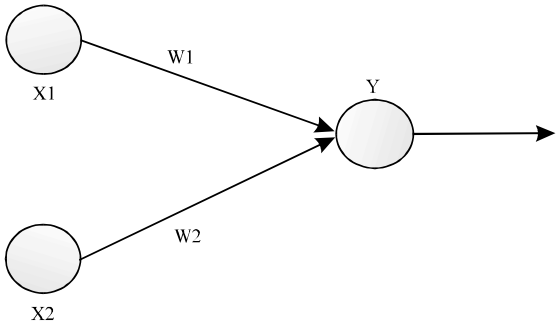

Fig. 6: Pictorial representation of a simple artificial neural network

noisy environment (Soares *et al*., 2009; Haykin, 1998). The foremost purpose of the neural network is to transfer the information with the help of interconnected neurons same like the biological cells in the brain. These neurons are interrelated by a large number of weighing links and with the help of this signals can pass (Haykin, 1998) (Fig. 6-8).

Neurons contain several signals viva incoming connections and produce a single output. It contains some key applications like pattern recognition or data classification through the learning process. It has great speed of transferring the information owing to their highly massive parallelism. The following given block diagram defines the whole picture of artificial neural network applications (Sivanandam *et al*., 2006). Basically, ANN is considered as a computing model same as the brain of human being and system of nervous. ANN has the capability for learning, saving and making relevance between input and output layer. ANN is a dynamic option because it contains a precision of predication adequately as compare to other traditional techniques (Haykin, 1998).

Attributes and identification of ANN Models: Generally, the architecture of ANN consists of three

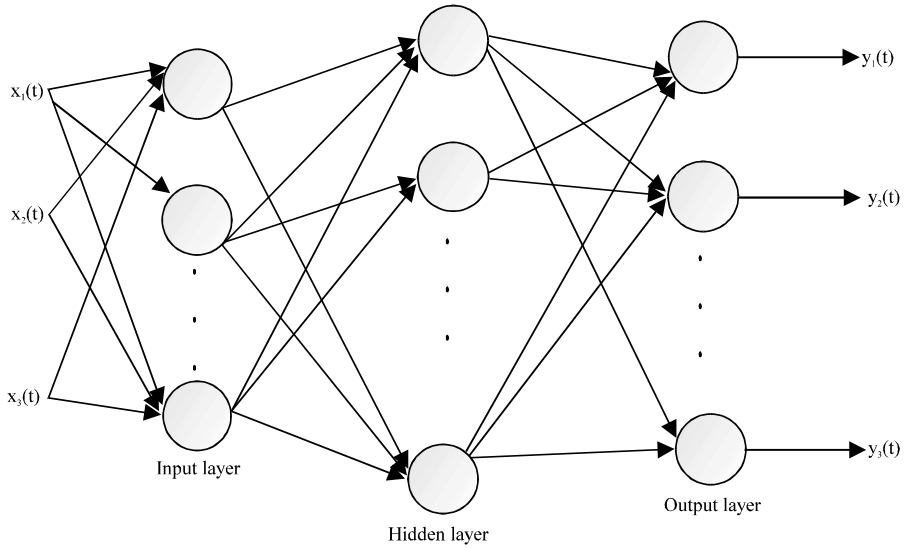

Fig. 7: Pictorial representation of an interlinked three-layered neural network. Each circle characterizes as an artificial neuron

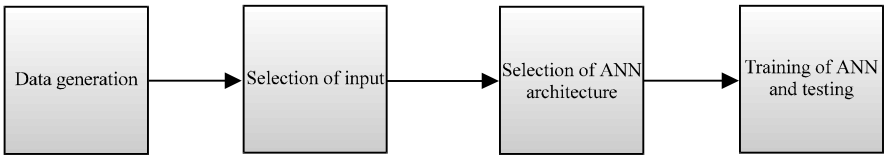

Fig. 8: Block diagram representation of the necessary steps of the ANN applications

layers which are shown in the above figures. Every layer has a specific task which described (Yu *et al*., 2016):

Input layer: The main purpose of the input layer to connect with the exterior environment. The pattern which is presented by the input layer is totally different from that pattern which is produced by the output pattern. Another research of input layer to generate the condition for training the neural network.

Output layer: The purpose of the output layer to produce a pattern for the exterior environment, the research where the neural network is to performed and the layer of output must be connected.

Hidden layer: Hidden layer is the intermediate stage of the neural network. It is the combination of hidden neurons which neither lies on the input layer nor the output layer. A mathematical expression is represented in "Eq. 2" which completely described the attributes of the ANN Models:

$$X_H = \sum_{k=1}^{k=m} W_{hk} i_k + W_{hb} b_i \quad (2)$$

Where:

W_{hk} = Weighing variable amid input and hidden layer
W_{hb} = Weighing variable amid hidden and bias node of the input layer
b = Bias node of the input layer
I = Input node
X_H = Collected input

Network classifications: The main aim of providing several network classification of ANN to resolving a problem and providing information engineering. Following network types are used in ANN (Sivanandam *et al*., 2006; Yu *et al*., 2016):

- Multi layer perceptron
- Single-layer perceptron
- Feedforward neural network
- Recurrent neural network
- Radial basis function network

Network activation functions

Mean Square Error (MSE): The value of MSE should be very small at the end of the training phase, so that, the desired output and output came from the ANN controller have become very near to each other. The expression of the MSE is presented in "Eq. 3":

$$MSE = \frac{\sum_{i}^{n}(O_i - O_m)^2}{n} \quad (3)$$

Where:

O_i = Real Output values
O_m = Forecasted Output values
I = Training vectors
N = Whole values of training

Root Mean Square Error (RMSE): The usage of RMSE is to measure the performance of the neural network. The expression of RMSE is given in "Eq. 4":

$$RMSE(\%) = \sqrt{\frac{(\sum_{1}^{n}(O_n - O_m))}{(n-1)}} \quad (4)$$

Where:

O_n = Measured Output value
n = Training patterns number

Mean Absolute Error (MAE): The main purpose of MAE is to make filtering in the utmost expected optimum networks in two situations, training and checking data sets. The expression of MAE is presented below in "Eq. 5" and the typical values of MAE and RMSE are zero or inclines to zero:

$$MAE = \frac{\sum_{i=1}^{n}|O_n - O_m}{n} \quad (5)$$

The coefficient of correlation (R^2): It is used for checking the predictions of output accuracy level. The selection of the best and right neural network is done by given "Eq. 6":

$$R^2 = 1-\sqrt{\frac{\sum_{1}^{n}|(O_n - O_m)|}{O_n}} \quad (6)$$

Standardizing and normalized data: Sigmoidal transfer function which has been specified by input and hidden layers is commonly used to develop the relationship between complex and nonlinear values is shown in "Eq. 7":

$$G(X_u) = \frac{e^{X_u}}{1+e^{X_u}} \quad (7)$$

where, X_u = weighted algebraic summation of inputs and:

$$X_j = \frac{\min(X_n) - X_{nj}}{\min(X_n) - \max(X_n)} \quad (8)$$

Where:

X_n = $(X_{n1}, ..., X_{nm})$
X_j = Ith standardized data
X_{nj} = The ith input data that need to standardize it

Dynamic modelling of DFIG: The voltage expressions of the stator and rotor of the Doubly-Fed Induction Generator (DFIG) in the arbitrary reference frame are presented in matrix configuration in "Eq. 9" and 10" (Boldea and Nasar, 2001):

$$\begin{bmatrix} v_{ds} \\ v_{qs} \end{bmatrix} = R_s \begin{bmatrix} 1 & 0 \\ 0 & 1 \end{bmatrix} \begin{bmatrix} i_{ds} \\ i_{qs} \end{bmatrix} + D \begin{bmatrix} \psi_{ds} \\ \psi_{qs} \end{bmatrix} + \omega_e \begin{bmatrix} 0 & -1 \\ 1 & 0 \end{bmatrix} \begin{bmatrix} \psi_{ds} \\ \psi_{qs} \end{bmatrix} \quad (9)$$

$$\begin{bmatrix} v_{dr} \\ v_{qr} \end{bmatrix} = R_r \begin{bmatrix} 1 & 0 \\ 0 & 1 \end{bmatrix} \begin{bmatrix} i_{dr} \\ i_{qr} \end{bmatrix} + D \begin{bmatrix} \psi_{dr} \\ \psi_{qr} \end{bmatrix} + (\omega_e - P\omega_r) \begin{bmatrix} 0 & -1 \\ 1 & 0 \end{bmatrix} \begin{bmatrix} \psi_{dr} \\ \psi_{qr} \end{bmatrix} \quad (10)$$

$$T_e = 1.5P \begin{bmatrix} \psi_{ds} & \psi_{qs} \end{bmatrix} \begin{bmatrix} i_{qs} \\ -i_{ds} \end{bmatrix} \quad (11)$$

where, in the above given all expressions, all currents (i) and voltages (v) refer to the arbitrary reference frame. The subscripts, dr, qr, ds and qs relate to d and q-axis quantities for the rotor (r) and stator (s) in whole combinations. ψ symbolizes as flux linkage. ω_e and ω_r are the speed of the reference frame and the mechanical speed of the rotor in rad/sec. R_r and R_s are rotor and stator resistance per phase correspondingly. Here, P is considered as the number of pole pairs and assuming (D = d/dt). Now, taking the assumption that the magnetic circuit is linear and the value of mutual inductance is equal as well as core loss (iron) is also neglected. Then, the expressions of flux linkage in matrix configuration are given below in "Eq. 12". And "Eq. 13" (Hamad and Ahmed, 2015):

$$\begin{bmatrix}\psi_{ds}\\ \psi_{qs}\end{bmatrix}=L_s\begin{bmatrix}1 & 0\\ 0 & 1\end{bmatrix}\begin{bmatrix}i_{ds}\\ i_{qs}\end{bmatrix}+L_m\begin{bmatrix}1 & 0\\ 0 & 1\end{bmatrix}\begin{bmatrix}i_{dr}\\ i_{qr}\end{bmatrix} \quad (12)$$

$$\begin{bmatrix}\psi_{dr}\\ \psi_{qr}\end{bmatrix}=L_m\begin{bmatrix}1 & 0\\ 0 & 1\end{bmatrix}\begin{bmatrix}i_{ds}\\ i_{qs}\end{bmatrix}+L_r\begin{bmatrix}1 & 0\\ 0 & 1\end{bmatrix}\begin{bmatrix}i_{dr}\\ i_{qr}\end{bmatrix} \quad (13)$$

In the "Eq. 12" and 13 L_r and L_s are illustrated as self-inductance of rotor and stator correspondingly and L_m is the mutual inductance between stator and rotor. Where, $L_s = L_m+L_{ls}$ and $L_r = L_m+Ll_r$. Now, the expression of current is given in "Eq. 14" and 15":

$$\begin{bmatrix}i_{qs}\\ i_{qr}\end{bmatrix}=\frac{1}{L_sL_r-L_m^2}\begin{bmatrix}L_r & -L_m\\ -L_m & L_s\end{bmatrix}\begin{bmatrix}\psi_{qs}\\ \psi_{qr}\end{bmatrix} \quad (14)$$

$$\begin{bmatrix}i_{ds}\\ i_{dr}\end{bmatrix}=\frac{1}{L_sL_r-L_m^2}\begin{bmatrix}L_r & -L_m\\ -L_m & L_s\end{bmatrix}\begin{bmatrix}\psi_{ds}\\ \psi_{dr}\end{bmatrix} \quad (15)$$

Now, the state space model of the DFIG in terms of stator and rotor flux linkages is given in "Eq 16":

$$D\begin{bmatrix}\psi_{qs}\\ \psi_{ds}\\ \psi_{qr}\\ \psi_{dr}\end{bmatrix}=A\begin{bmatrix}\psi_{qs}\\ \psi_{ds}\\ \psi_{qr}\\ \psi_{dr}\end{bmatrix}+I\begin{bmatrix}v_{qs}\\ v_{ds}\\ v_{qr}\\ v_{dr}\end{bmatrix} \quad (16)$$

Here:

$$A=\begin{bmatrix}-b_1 & -\omega_e & b_2 & 0\\ \omega_e & -b_1 & 0 & b_2\\ b_3 & 0 & b_4 & (\omega_e-P\omega_r)\\ 0 & b_3 & (\omega_e-P\omega_r) & -b_4\end{bmatrix} \text{ and } I=\begin{bmatrix}1 & 0 & 0 & 0\\ 0 & 1 & 0 & 0\\ 0 & 0 & 1 & 0\\ 0 & 0 & 0 & 1\end{bmatrix}$$

In the matrix A:

$$b_1=\frac{R_s}{\sigma L_s},\ b_2=\frac{R_sL_m}{\sigma L_sL_r},\ b_3=\frac{R_rL_m}{\sigma L_sL_r},\ b_4=\frac{R_r}{\sigma L_r} \text{ and } \sigma=\frac{L_sL_m-L_m^2}{L_sL_r} \text{ is}$$

delineated as a leakage coefficient. Again the state space model of the DFIG in terms of rotor current and stator flux linkages is given in "Eq. 17".

$$D\begin{bmatrix}\psi_{qs}\\ \psi_{ds}\\ i_{qr}\\ i_{dr}\end{bmatrix}=B\begin{bmatrix}\psi_{qs}\\ \psi_{ds}\\ i_{qr}\\ i_{dr}\end{bmatrix}+C\begin{bmatrix}v_{qs}\\ v_{ds}\\ v_{qr}\\ v_{dr}\end{bmatrix} \quad (17)$$

Here:

$$B=\begin{bmatrix}-\alpha_1 & -\omega_e & 0 & \alpha_2\\ \omega_e & -\alpha_1 & \alpha_2 & 0\\ 0 & -\alpha_3 & \alpha_4 & -\omega_{sl}\\ -\alpha_3 & 0 & \omega_{sl} & -\alpha_4\end{bmatrix} \text{ and } C=\begin{bmatrix}1 & 0 & 0 & 0\\ 0 & 1 & 0 & 0\\ 0 & 0 & \alpha_5 & 0\\ 0 & 0 & 0 & \alpha\end{bmatrix}$$

In the matrix B and C:

$$\alpha_1=\frac{R_s}{L_s}\alpha_2=\frac{R_sL_m}{L_s}\alpha_3=\frac{\omega_{sl}L_m}{\sigma L_rL_s}\alpha_4=\frac{R_r}{\sigma L_r}\alpha_5=\frac{1}{\sigma L_r}$$

MATERIALS AND METHODS

Reactive power and DC bus voltage control (grid side control strategy): The vital motive of the implementation of grid side converter is to control the voltage of the DC bus capacitor. For grid side regulator, the positive sequence of the grid voltage is aligned with d-q transformation and this transformation uses the d-axis rotating reference frame. The q and d-axis of AC current which is to be controlled and the value of the voltage across the DC bus (DC) is measured by the measuring system which is regulated by the GSC (Hamatwi *et al*., 2016). Basically, grid side converter embraces two control loops, the first one is an inner loop which is known as the current controller and the second one is an outer loop which is known as DC voltage controller. The q-axis current is controlled by the interior loop by the means of ANN controller and the voltage across the DC-link capacitor is controlled by the external loop by the means of second ANN controller (Ekanayake *et al*., 2003).

To keep the constant value of the voltage across DC bus capacitor gives the assurance of the unity power factor operation of the converter and this will also ensure that only reactive power will exchange through the stator. The Grid Side Converter (GSC) control arrangement is displayed in "Fig. 9 and 10" (Hamatwi *et al*., 2016; Ekanayake *et al*., 2003; Mishra, 2018). In the DC bus, the voltage expression is given as:

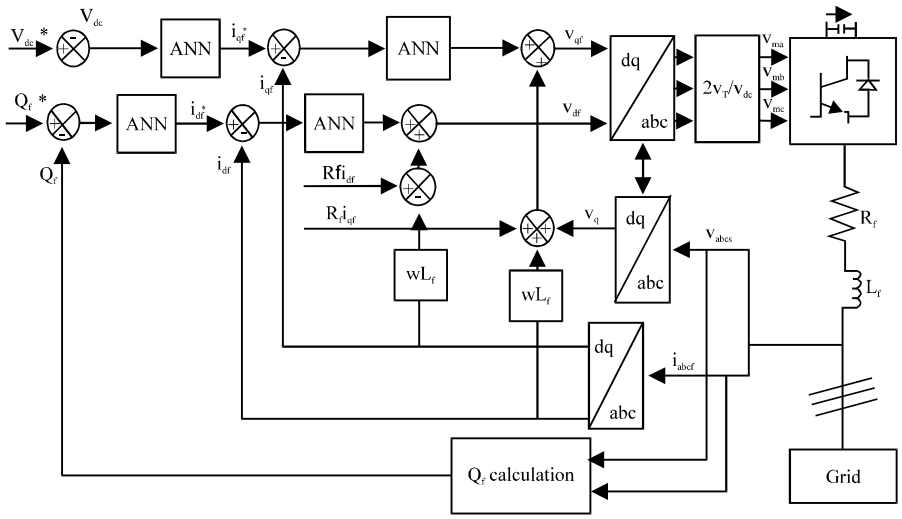

Fig. 9: Pictorial representation of grid side converter control strategy

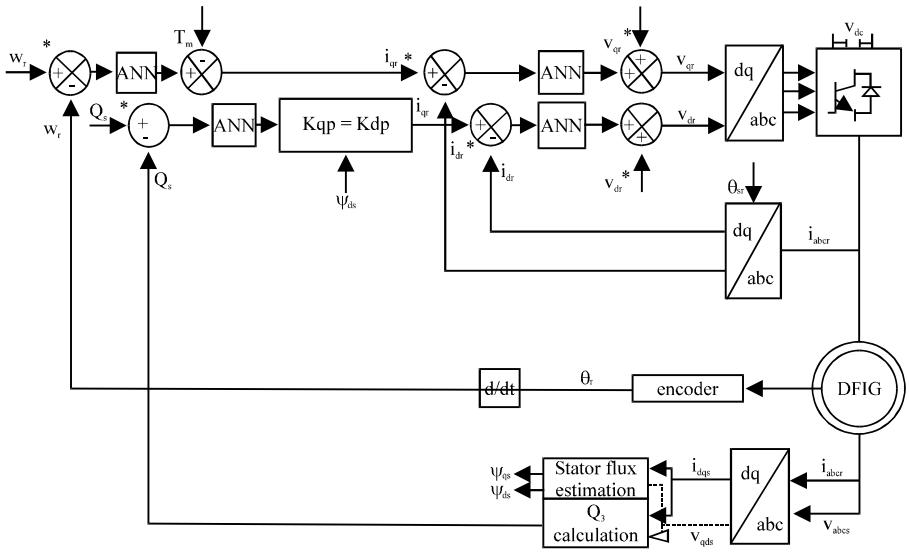

Fig. 10: Pictorial representation of block diagram of Rotor Side Control (RSC) strategy

$$C_{dc}Dv_{dc} = 0.75(m_{df}i_{df}+m_{qf}i_{qf}+m_{dr}i_{dr}+m_{qr}i_{qr}) \quad (18)$$

Where:

C_{dc} = Capacitance of the DC bus
m_{df} = GSC modulation index in q-axis
m_{df} = GSC modulation index in d-axis
m_{dr} = RSC modulation index in d-axis
m_{qr} = RSC modulation index in q-axis
D = First derivative (d/dt) throughout the paper

"Equation 18" can be remodified which is presented in "Eq. 19":

$$\sigma_{dc} = 0.75(m_{df}i_{df}+m_{qf}i_{qf}+m_{dr}i_{dr}+m_{qr}i_{qr}) = C_{dc}Dv_{dc} \quad (19)$$

From "Eq. 19", q-axis grid current is given:

$$i_{qf}^{*} = 1.33\frac{1}{m_{qf}}\left(\sigma_{dc}-0.75\left(m_{qr}i_{qr}+m_{dr}i_{dr}\right)\right)-\frac{m_{df}}{m_{qf}}i_{df} \quad (20)$$

By using KVL across the RL filter which gives the expressions of q and d-axis voltages of the grid side in "Eq. 21 and 22:

$$v_{qf} = R_f i_{qf} + L_f Di_{qf} + \omega_e L_f i_{df} + \frac{v_{qs}}{N_T} = 0.5 m_{qf} v_{dc} \quad (21)$$

$$v_{df} = R_f i_{df} + L_f Di_{df} - \omega_e L_f i_{qf} = 0.5 m_{df} v_{dc} \quad (22)$$

The reactive power supplied by grid side converter using the condition that $v_{ds} = 0$ and $v_{qs} = v_s$ is given as:

$$Q_f = \frac{1.5}{N_T} i_{df} v_s \quad (23)$$

In "Eq. 23", N_T is illustrated as the turns ratio of the transformer connected between stator and GSC:

$$DQ_f = 1.5\, Di_{df} \frac{v_s}{N_T} \quad (24)$$

After substituting the "Eq. 22" in "Eq. 24":

$$DQ_{ff} = 1.5\, Di_{df} \frac{v_s}{N_T L_f} \left(v_{df} - R_f i_{df} + \omega_e L_f i_{qf} \right) \quad (25)$$

$$\gamma DQ_f = \left(v_{df} - R_f v_{df} + \omega_e L_f i_{qf} \right) = \sigma_{Qf} \quad (26)$$

In "Eq. 26" $\gamma = 0.67 L_f N_T / v_s$ from "Eq. (26)", d-axis grid current is given:

$$i_{df}^* = \frac{1}{R_f} (v_{df} + \omega_e L_f i_{qf} - \sigma_{Qf}) \quad (27)$$

From the inner current regulation of the grid side converter:

$$R_f i_{qf} + L_f Di_{qf} = K_{qf} (i_{qf}^* - i_{qf}) = \sigma_{qf} \quad (28)$$

$$R_f i_{df} + L_f Di_{df} = K_{qf} (i_{df}^* - i_{df}) = \sigma_{df} \quad (29)$$

From the Eq. 18 and 19 modulation indexes of grid side in d-and q- axis is given as:

$$m_{qf} = \frac{2}{v_{dc}} (\sigma_{qf} + \frac{v_{qs}}{N_T} + \omega_e L_f i_{df}) \quad (30)$$

$$m_{df} = \frac{2}{v_{dc}} (\sigma_{df} - \omega_e L_f i_{qf}) \quad (31)$$

Active and reactive power control (rotor side control strategy): In rotor side control strategy, d and q axis currents are used to control the reactive and real power of the stator (Yang *et al*., 2007). As the stator voltage vector is aligned to the q-axis of rotating reference frame due to this the stator voltage across the d-axis (v_{ds}) is equal to zero and the stator voltage across the q-axis (v_{ds}) is equal to v_s. Stator side flux is controlled by the controller which is used in the rotor side and in this consideration ψ_{ds} is equal to ψ_s and ψ_{qs} is equal to 0 (Vas, 1990; Devashish and Thakur, 2017; Kumar and Singh, 2018). Now for both control of real and reactive power all the expressions are given below. The Rotor Side Converter (RSC) control arrangement is displayed below in "Fig. 10" (Hamatwi *et al*., 2016; Ekanayake *et al*., 2003; Mishra, 2018):

$$\begin{cases} D\psi_{qs} + b_1 \psi_{qs} = v_{qs} + b_2 \psi_{qr} - \omega_e \psi_{ds} \\ \sigma_{\psi qs} = v_{qs} + b_2 \psi_{qr} - \omega_e \psi_{ds} \\ \psi_{ds}^* = \frac{1}{\omega_e} (v_{qs} + b_2 \psi_{qr} - \sigma_{\psi qs}) \end{cases} \quad (32)$$

$$\begin{cases} D\psi_{ds} + b_1 \psi_{ds} = v_{ds} + \omega_e \psi_{qs} + b_2 \psi_{dr} \\ \sigma_{\psi ds} = v_{ds} + \omega_e \psi_{qs} + b_2 \psi_{dr} \\ \psi_{qs}^* = \frac{1}{\omega_e} (\sigma_{\psi ds} - b_2 \psi_{dr} - v_{ds}) \end{cases} \quad (33)$$

Substituting $\psi_{qs} = 0$ in Eq. 11 and 12 results in Eq. 34:

$$\begin{cases} T_{em} = 1.5 \psi_{ds} i_{qs} \\ i_{qs} = -\frac{L_m}{L_s} i_{qr} \end{cases} \quad (34)$$

From "Eq. 32", we get:

$$T_{em} = 1.5 \psi_{ds} (-\frac{L_m}{L_S}) i_{qr} \quad (35)$$

$$i_{qr} = 0.67 \left(\frac{\sigma_{\omega r} . L_s}{\psi_{ds} L_m} - \frac{T_m L_s}{\psi_{ds} L_m} \right) \quad (36)$$

Now, the active power supplied by stator is given as:

$$P_s = 1.5 (v_{qs} i_{qs} + v_{ds} i_{ds}) \quad (37)$$

Putting $v_{ds} = 0$ and the value of i_{qs}, we get:

$$P_s = -1.5 \frac{L_m}{L_s} v_{qs} i_{qr} \quad (38)$$

Now, the reactive power supplied by stator is given as:

$$Q_s = 1.5(v_{qs}i_{ds} - v_{ds}i_{qs}) \quad (39)$$

Putting the value of v_{ds} and v_{qs} in "Eq. 39":

$$Q_s = 1.5v_{qs}i_{ds} \quad (40)$$

$$Q_s = 1.5(R_s i_{qs} + \omega_e \psi_{ds} + s\psi_{qs})i_{ds} \quad (41)$$

Putting the value of i_{ds} from the "Eq. 15" in "Eq. 41" and neglect the resistance of stator by keeping the stator flux constant:

$$Q_s = 1.5(\psi_{ds}^2 - \frac{L_m}{L_r}\psi_{ds}\psi_{dr})\frac{\omega_e}{\sigma L_s} \quad (42)$$

Differentiating "Eq. 42" w. r. t. time provides:

$$DQ_s = -1.5\frac{\omega_e}{\sigma L_s}\frac{L_m}{L_r}\psi_{ds}D\psi_{dr} \quad (43)$$

The expression of ψ_{qr} in the terms of i_{qr} from "Eq. (41)" and " Eq. (10)":

$$\begin{cases} DQ_s = -1.5\frac{\omega_e}{\sigma L_s}\frac{L_m}{L_r}\psi_{ds}(v_{dr} + (\omega_e - \omega_r)\psi_{qr} - R_r i_{dr}) \\ DQ_s = -1.5\frac{\omega_e}{\sigma L_s}\frac{L_m}{L_r}\psi_{ds}(v_{dr} + (\omega_e - \omega_r)\sigma L_r i_{qr} - R_r i_{dr}) \\ \varepsilon DQ_s = (Q_s^* - Q_s)K_{Qs} = \sigma_{Qs} \end{cases} \quad (44)$$

Where:

$$\varepsilon = \frac{0.67\, L_r L_s \sigma}{L_m \omega_e}$$

From "Eq. 43 and 44", d-axis rotor current is given:

$$i_{dr}^* = \frac{1}{R_r}(v_{dr} + \frac{\sigma_{Qs}}{\psi_{ds}} + \sigma L_r i_{qr}(\omega_e - \omega_r)) \quad (45)$$

The rotor side d and q axis voltages expression from the "Eq. (10-13)" is given:

$$v_{qr} = R_r i_{qr} + \omega_{sl}\left(\frac{L_m}{L_s}\psi_{ds} + \sigma L_r i_{dr}\right) + \sigma L_r D i_{qr} \quad (46)$$

Table 2: Network characters of ANN training window

Network types	Network characters
Inputs of the network	Rotor current in d-axis, rotor current in q-axis, speed of the rotor
The target of the network	Real power, reactive power, DC bus voltage
Training function	TRAINLM
Network configuration	Feed-forward backpropagation
Adjustment learning function	LEARNGDM
Function of performance	Mean Square Error (MSE)
Number of hidden layers	8

Table 3: Neural network training regression values

Processes	Regression values (R)
Training	0.9558
Validation	0.95449
Testing	0.953
All	0.95503

$$v_{dr} = R_r i_{dr} - \omega_{sl}\sigma L_r i_{qr} + \sigma L_r D i_{dr} \quad (47)$$

where, $\omega_{sl} = (\omega_e - \omega_r)$ is defined as a slip speed. Then the q-axis and the d-axis reference voltage of the rotor side are given as:

$$v_{qr}^* = \sigma_{qr} + \omega_{sl}(\frac{L_m}{L_s}\psi_{ds} + \sigma L_r i_{dr}) \quad (48)$$

$$v_{dr}^* = \sigma_{dr} - \omega_{sl}(\sigma L_r i_{qr}) \quad (49)$$

DFIG control strategy using ANN simulation model: In artificial neural network controller for training purpose, we selected by default Levenberg-Marquardt algorithm. The purpose of MATLAB Toolbox is to open the window of data manager of neural network and with the help of this, operator import, build and then export neural networks and data are produced. Following "Table 2 and 3". explained all network characters of my proposed research work.

A feed-forward neural network which contained two layers is used for fitting the function and hidden layer contained sigmoid transfer function and along with this, output layer embraced a linear transfer function. For updating the values of the weights and bias, Levenberg-Marquardt Back Propagation (BP) algorithm with output neurons (linear) and hidden neurons (sigmoid) as the activation functions used in an individual layer. The target vectors of the input will be categorized into three sets in random (dividend) form:

- About 70% of the first set-pattern training
- About 15% of the second set-validation of neural network generalization
- About 15% of the third set-independent testing of neural network generalization

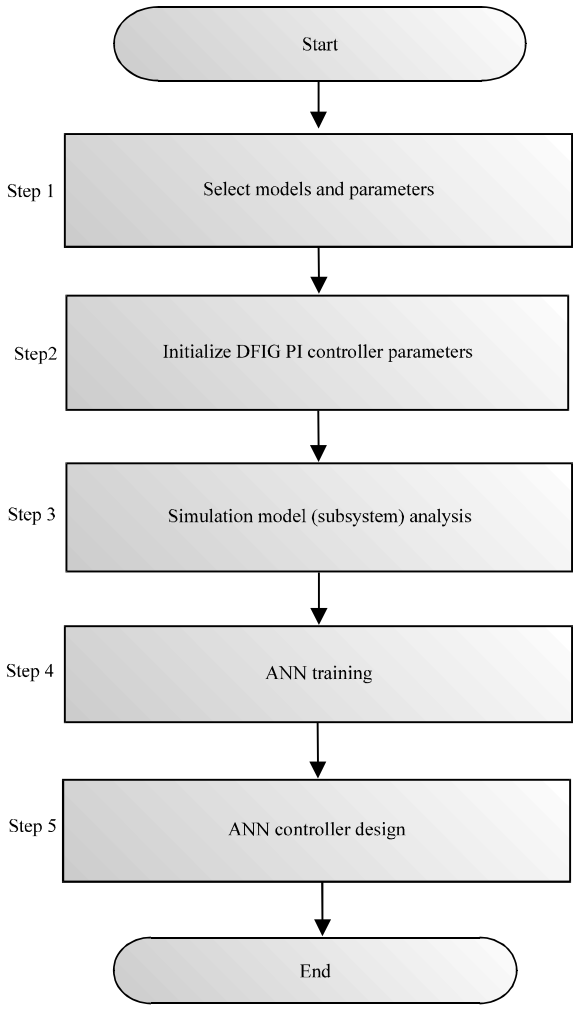

Fig. 11: Pictorial representation of a flowchart of ANN optimal DFIG Model design process

For reactive power control of rotor side, we used the 3-8-1 configuration of neural network. Where the number of input is 3, the number of hidden layers is 8 and the output is 1. In the input configuration, rotor current in d-axis (measured and reference) is used and in the output side, reactive power and the reference voltage are controlled. For active power control of rotor side, we again used 3-8-1 configuration of neural network. Where the number of input is 3, the number of hidden layers is 8 and the output is 1. In the input configuration, q-axis rotor current (reference and measured) and speed of the rotor is used and in the output side, active power of the rotor is controlled. "Table 3." presented the practical values which came during the training the neural network for this proposed research work. To concisely described the function of the ANN controller with DFIG, a complete flow chart is shown in "Fig. 11" (Sivanandam *et al*., 2006). This flow chart states the step by step work which has been done to complete this research work.

RESULTS AND DISCUSSION

After successfully implementation of ANN control techniques on the simulation model and all the simulated outcomes are analyzed in the terms of back to back converter rating and real and reactive power. All the subfigures of Fig. 16 are presented in the waveforms and these waveforms show the operation of 2 MW SHPP linked with 2 MW DFIG at different modes of speed (sub-synchronous to super synchronous viva synchronous mode). All the results in terms of DC link voltage, stator current frequency, rotor current frequency, rotor speed useful (real) power and reactive power are tabulated in Table 4 (Fig. 12-22).

Operation of DFIG at sub-synchronous mode: In this manner of operation, the speed of the rotor (rotor speed-125.6 rad/sec as shown in the waveform) is less as compared to reference speed (157 rad/sec), so, the value of slip is positive. Also, in this situation, line delivers power to the rotor circuit and DC bus voltage is preserved at a constant level to assured the zero power factor angle operation at the grid side. For validation of the operation, the waveforms of stator current, rotor current, supply voltage and DC bus voltage is presented.

Operation of DFIG at synchronous mode: In this manner of operation, the speed of the rotor (rotor speed-157 rad/sec as shown in the waveform) is same as reference speed (157 rad/sec), so, the value of slip is zero. Furthermore, in this style of operation, the DC bus voltage also at the grid side is maintained at a constant level to make the zero power factor angle operation. For validation of the process, the waveforms of stator current, rotor current, supply voltage and DC bus voltage is presented.

Operation of DFIG at super synchronous mode: In this manner of operation, the speed of the rotor (188.4 rad/sec as shown in the waveform) is more as compared to reference speed (157 rad/sec), so, the value of slip is negative. Moreover, in this style of operation, line gained power from the rotor circuit. Moreover, it can be undoubtedly perceived that useful power delivered by

Table 4: Description of the performance of 2 MW SHPP linked with 2 MW DFIG at different modes of speed operation (sub synchronous, synchronous and super synchronous speed)

Rotor speed (rad/sec) (ω_r)	Stator current frequency (I_{sf})(Hz)	Rotor current frequency (I_{rf})(Hz)	Output real power (P_{out})(MW)	Output reactive power(Q_{out})(MVar)	Bus voltage (V_{bus})(V)	Supply voltage (V_s)(V)	Grid reactive power (Q_g)(MVar)
125.6	50	10	-1.48	00	1150	690	00
157	50	00	-1.67	00			
1150	690	00					
188.4	50	-10	-1.86	00	1150	690	00

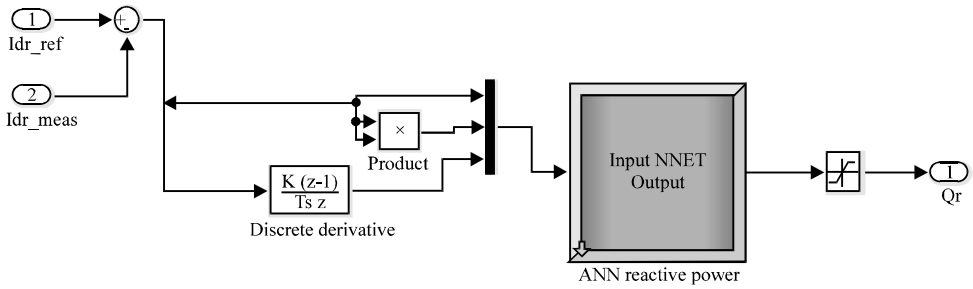

Fig. 12: Schematic representation of the ANN controller (Simulink Model) for reactive power control

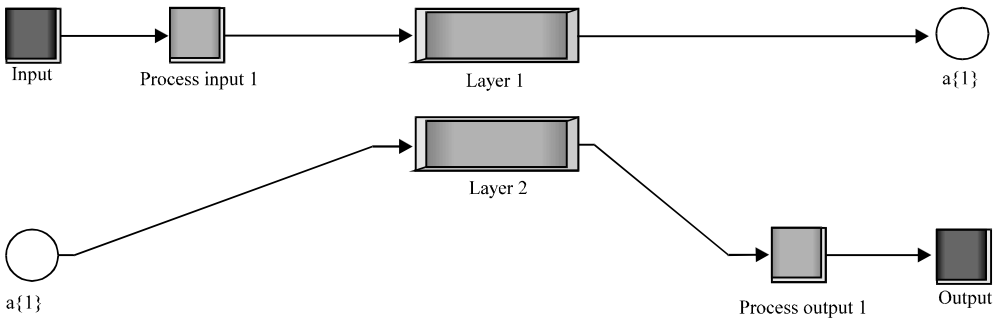

Fig. 13: An ANN layer model for reactive power control

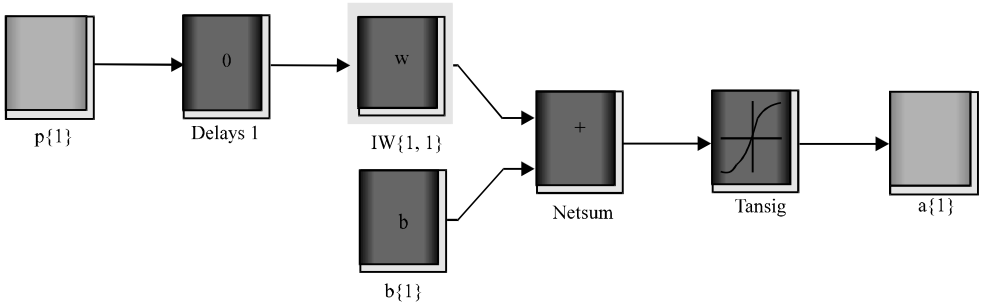

Fig. 14: Internal ANN layer (1) Model for reactive power control

DFIG is increasing from sub-synchronous mode to super synchronous mode as well as unity power factor operation is also observed in all three modes of operation. For validation of the action, the waveforms of stator current, rotor current, supply voltage and DC bus voltage is presented. A complete explanation of all simulated outcomes is presented below in the table format. From the "Table 4", it is concluded that as speed is increasing from 125.6-188.4 rad/sec viva synchronous speed 157 rad/sec, the output active power supplied from DFIG is also increasing. In all three manners of operation, DC bus voltage, supply voltage and stator current frequency are constant. The reactive power delivered from the rotor as well as the grid is zero.

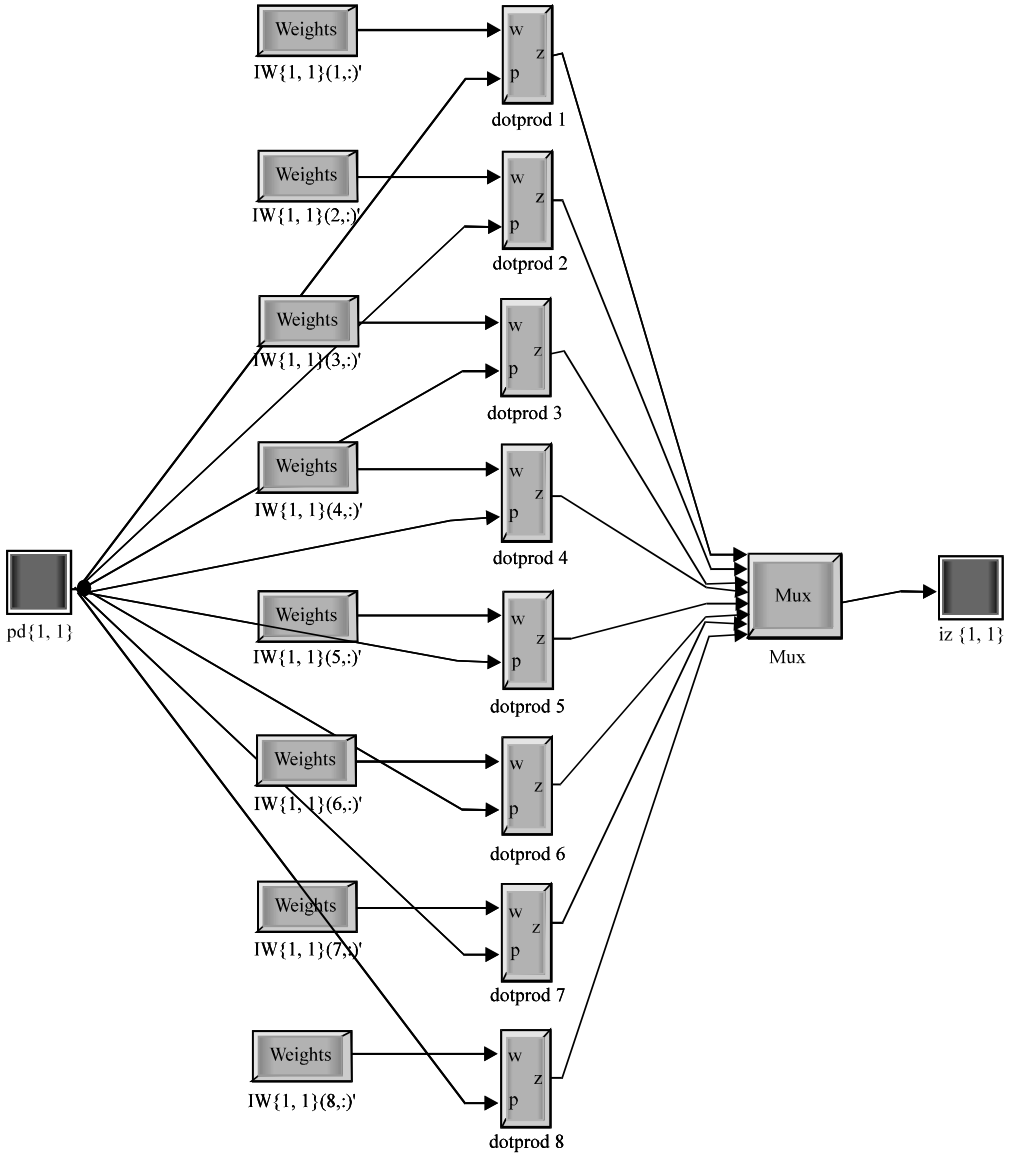

Fig. 15: Weights function of layer1 for reactive power

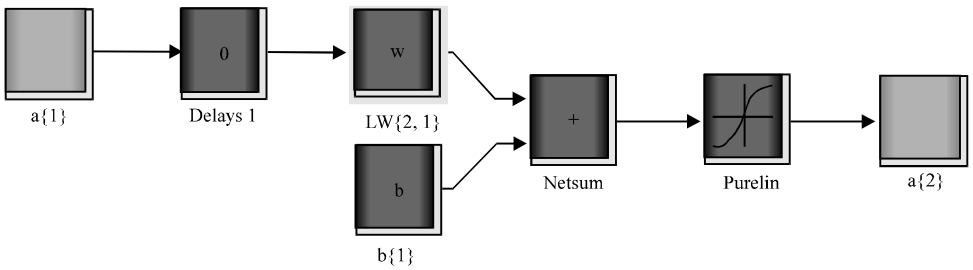

Fig. 16: Internal ANN layer (2) Model for reactive power

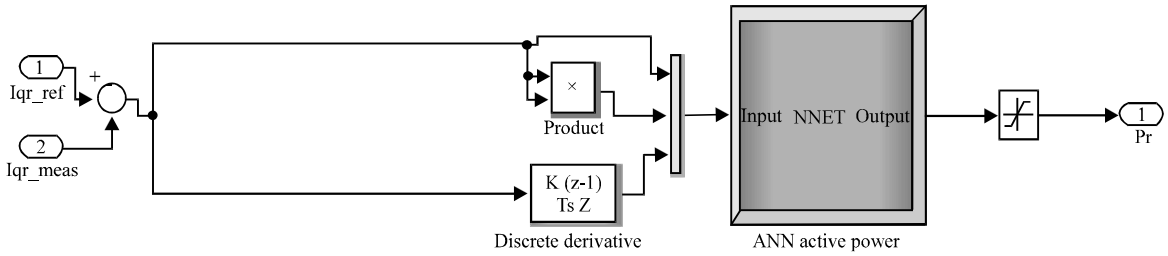

Fig. 17: Schematic representation of the ANN controller (Simulink Model) for active power control

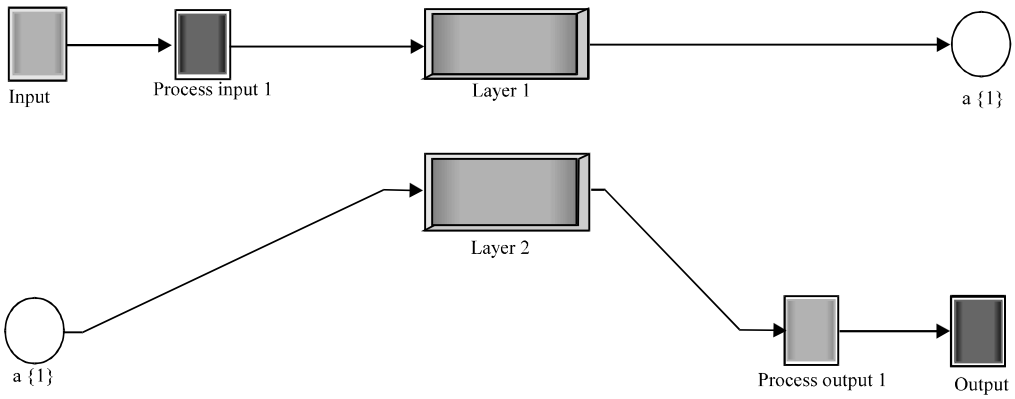

Fig. 18: An ANN layer model for active power control

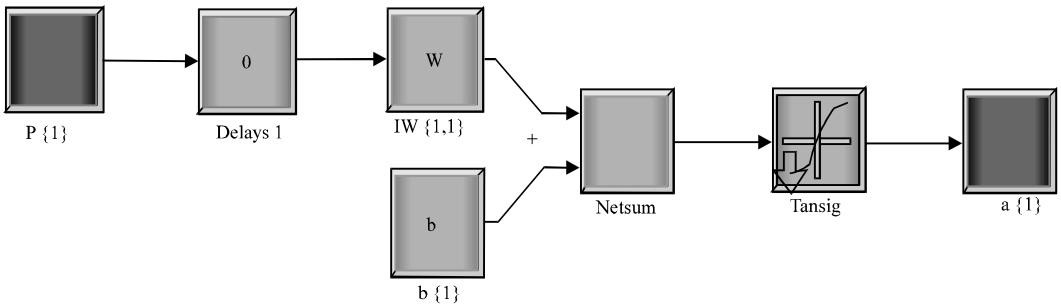

Fig. 19: Internal ANN layer (1) model for active power control

Table 5: The Parameters for 2 MW DFIG that have been used for designing the simulation model

Parameters	Values (Units)
Rated output power	2 (MW)
Frequency	50 (Hz)
Stator voltage	690 (Volt)
Stator/Rotor turns ratio	0.33 (-)
Pole Pairs	2 (-)
Rotor resistance	2.9 (mΩ)
Stator resistance	2.6 (mΩ)
Rotor inductance	2.58 (mH)
Stator inductance	2.58 (mH)
Mutual inductance	2.5 (mH)
Turbine rotor speed	157 (rad/sec)
Inertia constant	3.82 (sec)

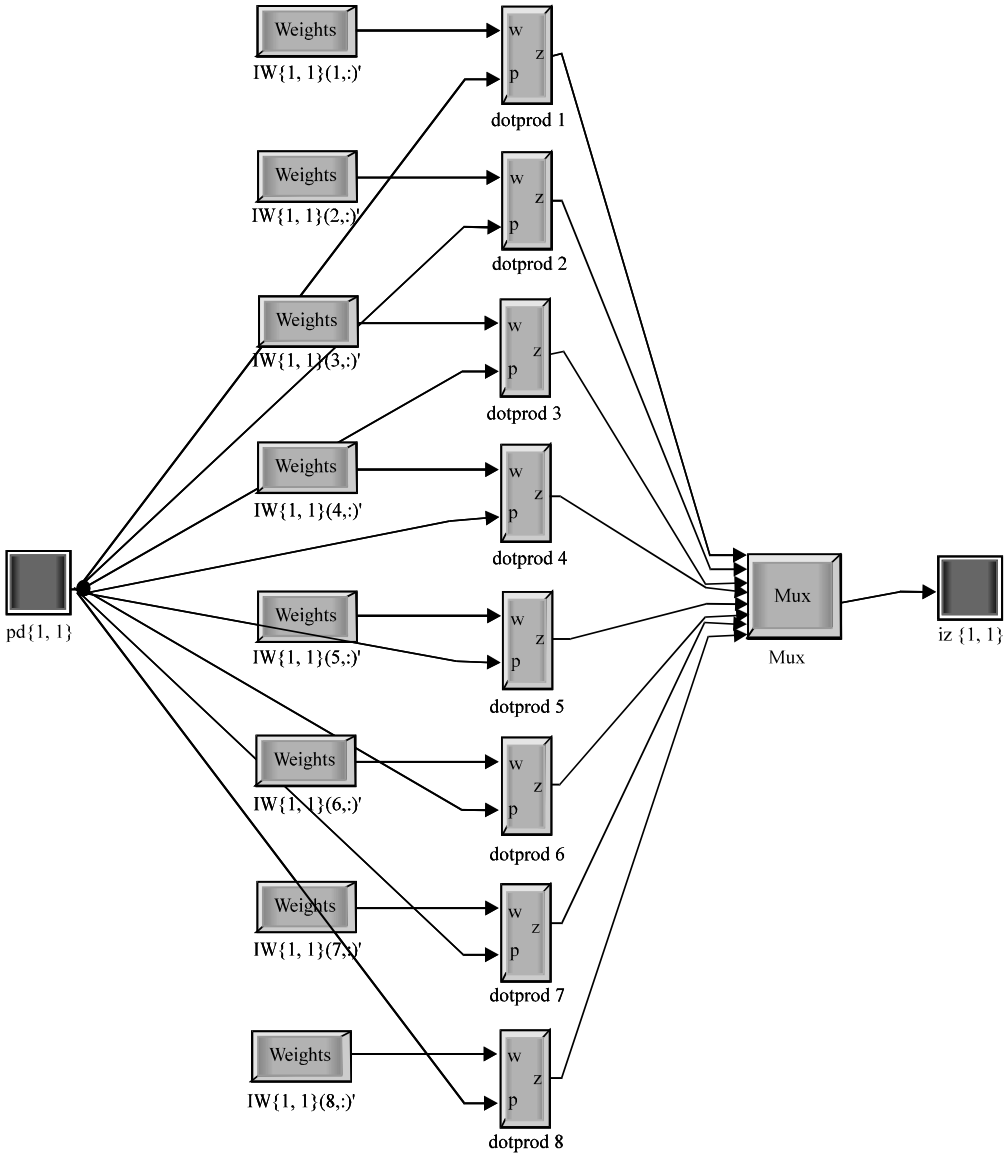

Fig. 20: Weights functions of layer (1) for active power control

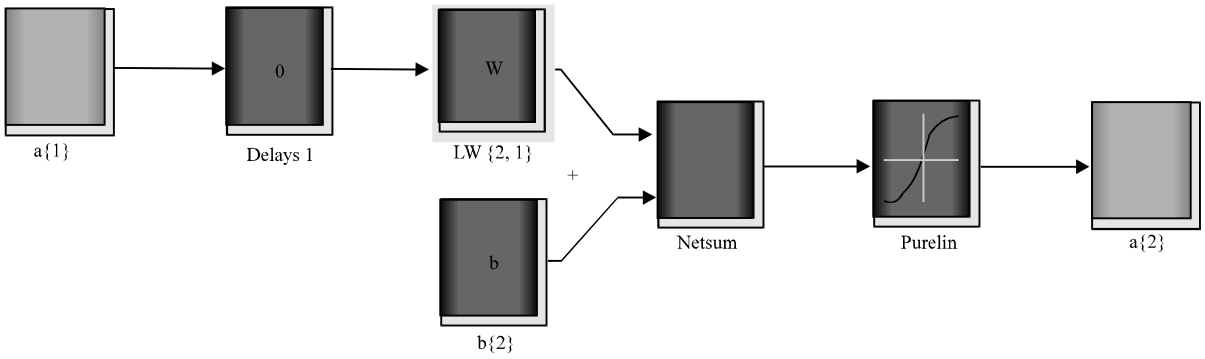

Fig. 21: Internal ANN layer (2) Model for active power control

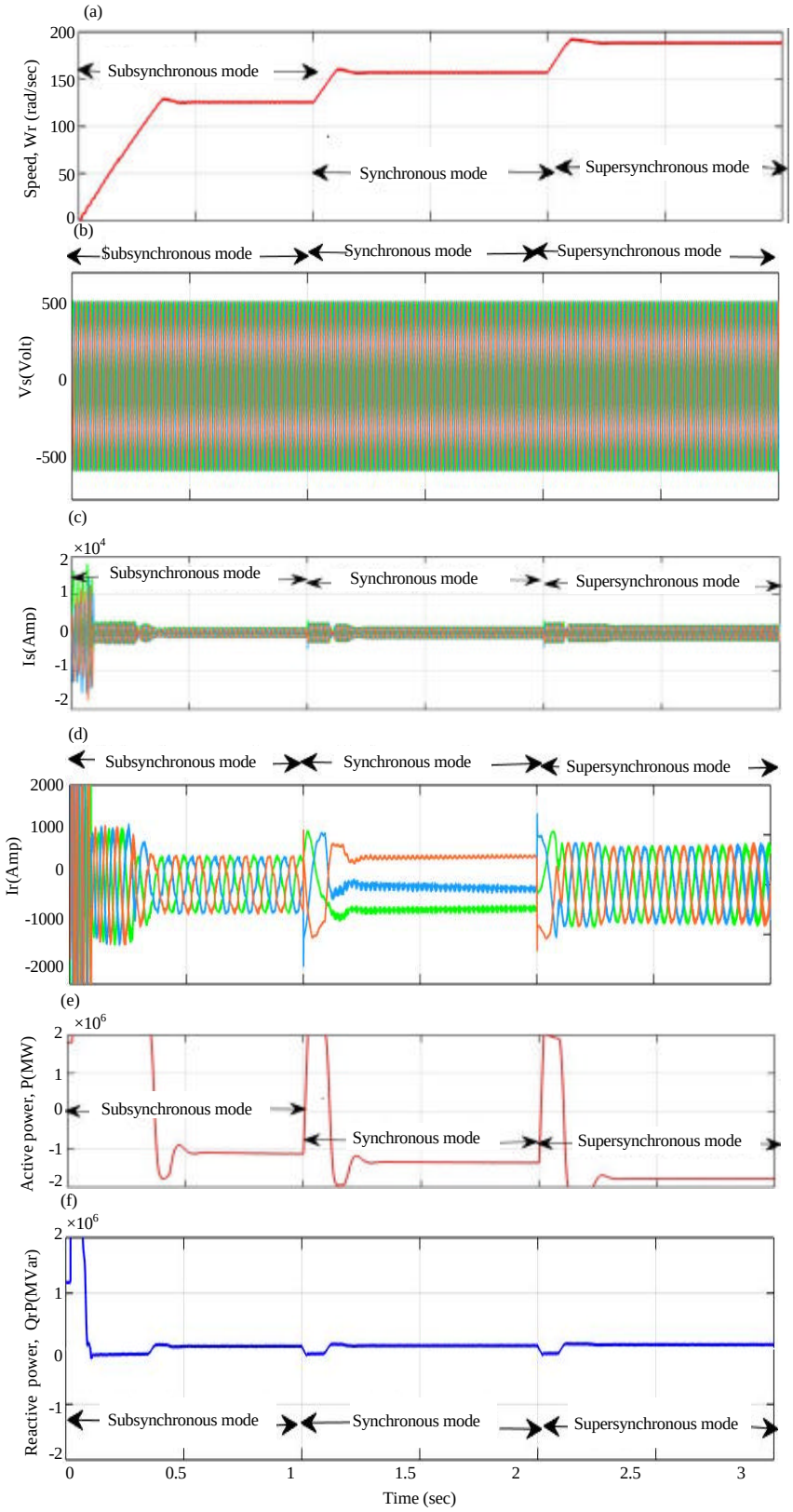

Fig. 22: Continue

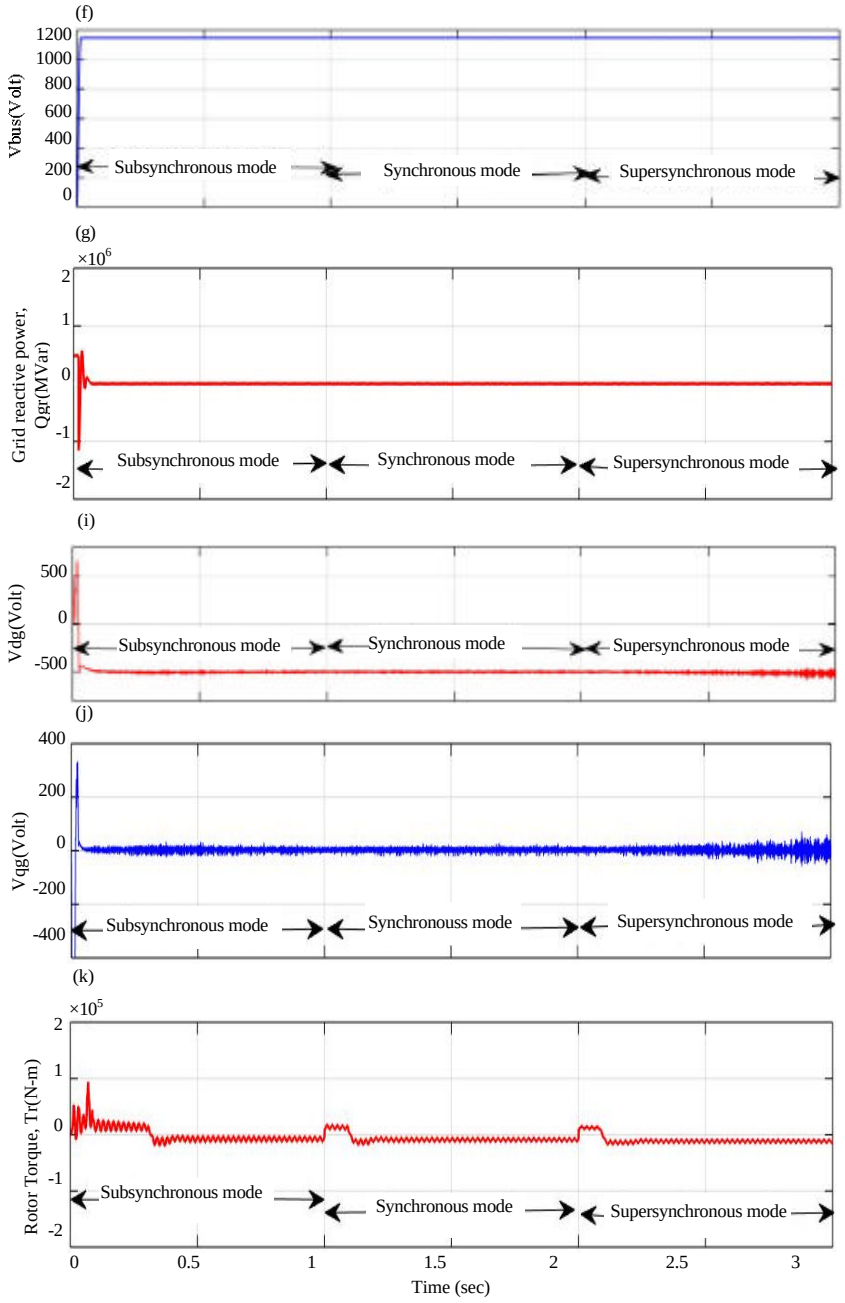

Fig. 22: a) Speed of the rotor; b) Stator voltage; c) Stator current; d) Rotor current; e) Active power; f) Rotor reactive power; g) DC bus voltage h) Reactive power at the grid side; i) Grid side d-axis voltage; j) Grid side q-axis voltage and k) Rotor torque

CONCLUSION

In this research work, the proposed Artificial Neural Network (ANN) control approach which has been efficaciously implemented for 2 MW Small HydroPower Plant (SHPP) associated with 2 MW Doubly Fed Induction Generator (DFIG) has ample of pros like good stabilization, less computational complication, real-time optimization as well as it does not require any mathematical model. On the other hand, it aids to abate the stress on power electronics converter which is built in DFIG and also abate the mechanical stress on the gearbox of hydraulic turbines. Time-domain simulation is used for verification of ANN approach which is applied

in DFIG. All the simulated outcomes delineate that the proposed model and control strategy, successfully and within very less time track the rotor reference speed to achieve the maximum power as well as sustain the dc bus voltage of the power converter at a constant level irrespective of instabilities due to variations in reactive and active power references. For unity power factor operation in grid side, the ANN controller sets the reactive in the grid side at a zero level. For a real-time application, we can use same presented simulation model in Real-Time digital simulator (RT-LAB) or Digital Signal Processor (DSP), so, the simulated outcomes acquired from ANN controller schemes and the simulated outcomes form RT-LAB or DSP is very much similar and undoubtedly acceptable in the real-time application.

ACKNOWLEDGEMENT

This research work was endorsed by National Institute of Technology, Jamshedpur, India. The first and second researchers is obliged to associate professor Dr. Madhu Singh (NIT, Jamshedpur) for endless guidance to complete this research work.

REFERENCES

Angela, L., 2008. Object-oriented modeling and simulation of Kaplan turbines. Master Thesis, KTH Royal Institute of Technology, Stockholm, Sweden.

Anonymous, 2017. The national electricity plan. The Government of India, Ministry of New and Renewable Energy, New Delhi, India.

Boldea, I. and S.A. Nasar, 2001. The Induction Machine Handbook. Taylor and Francis, Milton Park, Didcot, UK., ISBN:9780849300042, Pages: 968.

Boldea, I., 2005. Variable Speed Generators. 1st Edn., CRC Press, Boca Raton, Florida, USA., ISBN:9781420037265, Pages: 550.

Borges, C.L. and R.J. Pinto, 2008. Small hydro power plants energy availability modeling for generation reliability evaluation. IEEE. Trans. Power Syst., 23: 1125-1135.

Devashish and A. Thakur, 2017. A comprehensive review on wind energy system for electric power generation: Current situation and improved technologies to realize future development. Intl. J. Renewable Energy Res., 7: 1786-1805.

Ekanayake, J.B., L. Holdsworth, X. Wu and N. Jenkins, 2003. Dynamic modeling of doubly fed induction generator wind turbines. IEEE. Trans. Power Syst., 18: 803-809.

Ghumman, A.R., Y.M. Ghazaw, A.R. Sohail and K. Watanabe, 2011. Runoff forecasting by artificial neural network and conventional model. Alexandria Eng. J., 50: 345-350.

Hamad, M.S. and K.H. Ahmed, 2015. A multifunctional current source inverter control for wind turbine grid interfacing. Proceedings of the 2015 International Conference on Renewable Energy Research and Applications (ICRERA), November 22-25, 2015, IEEE, Palermo, Italy, pp: 1328-1331.

Hamatwi, E., I.E. Davidson and M.N. Gitau, 2016. Control of multi-level voltage source converters integrating a wind turbine system into the grid. Proceedings of the 2016 IEEE International Conference on Renewable Energy Research and Applications (ICRERA), Novmber 20-23, 2016, IEEE, Birmingham, UK., ISBN:978-1-5090-3389-8, pp: 813-819.

Haykin, S., 1998. Neural Networks: A Comprehensive Foundation. 2nd Edn., Prentice Hall, Upper Saddle River, New Jersey, USA., ISBN-13:978-0132733502, Pages: 842.

Iov, F., M. Ciobotaru and F. Blaabjerg, 2008. Power electronics control of wind energy in distributed power systems. Proceedings of the 2008 11th International Conference on Optimization of Electrical and Electronic Equipment, May 22-24, 2008, IEEE, Brasov, Romania, ISBN:978-1-4244-1544-1, pp: 29-44.

Khan, R., 2015a. Small hydro power in India: Is it a sustainable business?. Appl. Energy, 152: 207-216.

Khan, R., 2015b. Towards realising social sustainability in the small hydropower sector in India: Opportunities for social innovations. Intl. J. Innovation Sustainable Dev., 9: 48-62.

Kothandaraman, C.P. and R. Rudramoorthy, 2007. Fluid Mechanics and Machinery. 2nd Edn., New Age International Pvt Ltd, Delhi, India, ISBN:9788122425581, Pages: 712.

Krishnan, R., 2001. Electric Motor Drives: Modeling, Analysis and Control. Prentice Hall, Upper Saddle River, New Jersey, USA., ISBN:9780130910141, Pages: 626.

Kumar, S. and M. Singh, 2018. Improved power quality cuk converter for variable speed BLDC motor drive. J. Eng. Appl. Sci., 13: 1275-1285.

Madawala, U.K., T. Geyer, J.B. Bradshaw and D.M. Vilathgamuwa, 2012. Modeling and analysis of a novel variable-speed cage induction generator. IEEE. Trans. Ind. Electron., 59: 1020-1028.

Madawala, U.K., T. Geyer, J.B. Bradshaw and D.M. Vilathgamuwa, 2012. Modeling and analysis of a novel variable-speed cage induction generator. IEEE. Trans. Ind. Electron., 59: 1020-1028.

Magureanu, R., M. Albu, V. Bostan, A.M. Dumitrescu and M. Pelizza *et al*., 2008. Optimal operation of Francis small hydro turbines with variabiable flow. Proceedings of the 2008 IEEE International Symposium on Industrial Electronics, June 30-July 2, 2008, IEEE, Cambridge, UK., ISBN:978-1-4244-1665-3, pp: 1562-1567.

Mishra, M.K., N. Khare and A.B. Agrawal, 2015. Small hydro power in India: Current status and future perspectives. Renewable Sustainable Energy Rev., 51: 101-115.

Mishra, S., 2018. Performance analysis of grid integrated doubly fed induction generator for small hydropower plant. Intl. J. Renewable Energy Res., 8: 2310-2323.

Perez, J.I., J.R. Wilhelmi and L. Maroto, 2008. Adjustable speed operation of a hydropower plant associated to an irrigation reservoir. Energy Conversion Manage., 49: 2973-2978.

REN21., 2015. Renewables 2015: Global Status Report. REN21 Secretariat Operates, Paris, France, ISBN:978-3-9815934-6-4, Pages: 251.

Sivanandam, S.N., S. Sumanthi and S.N. Deepa, 2006. Introduction to Neural Networks Using Matlab 6.0. Tata McGraw-Hill Publishing Company Ltd., New Delhi.

Soares, O.M., H.N. Goncalves, A.P. Martins and A.S. Carvalho, 2009. Analysis and NN-based control of doubly fed induction generator in wind power generation. Proceedings of the 2009 International Conference on Renewable Energies and Power Quality (ICREPQ'09) Vol. 1, April 15-17, 2009, Valencia, Spain, pp: 117-122.

Subramanya, K., 2013. Hydraulic Machines. 1st Edn., Mc Graw Hill India, Noida, India, ISBN:9781259006845, Pages: 599.

Vas, P., 1990. Vector Control of AC Machines. Clarendon Press, Wotton-under-Edge, England, ISBN:9780198593706, Pages: 332.

Yang, Z., Z. Xudong, H. Daocheng, L. Xinmin and C. Fengxiang *et al*., 2007. Research on excitation control of flexible power conditioner doubly fed induction machine. Proceedings of the 2007 International Conference on IEEE Power Electronics Specialists, June 17-21, 2007, IEEE, Orlando, Florida, USA., ISBN:978-1-4244-0654-8, pp: 92-97.

Yu, X., C. Ye and L. Xiang, 2016. Application of artificial neural network in the diagnostic system of osteoporosis. Neurocomputing, 214: 376-381.